Charged particle nonlinear resonance with localized electrostatic wave-packets

Artemyev A. V.[1,2], Vasiliev A. A.[2], Neishtadt A. I.[3,2]
[1] *Institute of Geophysics and Planetary Physics, University of California, Los Angeles, CA, USA,* [2] *Space Research Institute, Moscow, Russia,* [3] *Department of Mathematical Sciences, Loughborough University, Loughborough LE11 3TU, United Kingdom*
(Dated: January 16, 2019)

A resonant wave-particle interaction, in particular a nonlinear resonance characterized by particle phase trapping, is an important process determining charged particle energization in many space and laboratory plasma systems. Although an individual charged particle motion in the nonlinear resonance is well described theoretically, the kinetic equation modeling the long-term evolution of the resonant particle ensemble has been developed only recently. This study is devoted to generalization of this equation for systems with localized wave packets propagating with the wave group velocity different from the wave phase velocity. We limit our consideration to the Landau resonance of electrons and waves propagating in an inhomogeneous magnetic field. Electrons resonate with the wave field-aligned electric fields associated with gradients of wave electrostatic potential or variations of the field-aligned component of the wave vector potential. We demonstrate how wave-packet properties determine the efficiency of resonant particle acceleration and derive the nonlocal integral operator acting on the resonant particle distribution. This operator describes particle distribution variations due to interaction with one wave-packet. We solve kinetic equation with this operator for many wave-packets and show that solutions coincide with the results of the numerical integration of test particle trajectories. To demonstrate the range of possible applications of the proposed approach, we consider the electron evolution induced by the Landau resonances with packets of kinetic Alfven waves, electron acoustic waves, and very oblique whistler waves in the near-Earth space plasma.

PACS numbers: 52.35.-g, 52.20.Dq, 96.50.Fm

I. INTRODUCTION

Rapid development of experimental techniques for measurements of high-frequency electromagnetic fields in space plasmas in the last two decades provides a lot of evidences of large-amplitude coherent electromagnetic and electrostatics waves in the near-Earth space. Unlike the broad spectrum low amplitude waves occupying large coordinate and time domains, these large amplitude waves represent various solitary structures [e.g., electrostatic solitons, electron holes, double layers, and Langmuir wave-packets, see 1–8] and quite localized wave-packets including few wave lengths [e.g., kinetic Alfven pulses, whistler wave packets, and low-hybrid wave bursts, see 9–14]. Similar large amplitude wave bursts were reproduced in laboratory experiments [e.g., 15–18]. The resonant interaction of such waves with charged particles is essentially nondiffusive and includes nonlinear effects like phase trapping and phase bunching (scattering) [e.g., 19, 20, and references therein]. Therefore, there is an open question: how to describe the long-term evolution of the charged particle velocity distribution in the system with an ensemble of large amplitude localized waves?

The resonant wave-particle interaction is responsible for many important plasma processes, and is well described for many systems in the self-consistent frame. However, the near-Earth plasma environment is often characterized by two different particle populations, one of which contributes to wave generation and another one experiences a significant acceleration due to resonant interaction with generated waves. The first population is shaped by various external factors, quite complicate to be accurately modeled. Thus, the convenient approach for investigation of the resonant wave-particle interaction consists in collection of statistics of spacecraft observations of wave properties and using this statistics to derive global models calculating the particle acceleration without estimates of feedback of accelerated particles on waves [e.g.,reviews 21, 22, and references therein]. Resonant particles can affect the wave significantly [e.g., 23, 24]; however, such *test particle* approach sometime represents a reasonable simplification and allows to describe many space plasma phenomena [25–28]. The basic kinetic equation in this approach is the Fokker-Planck diffusion equation derived within the quasi-linear theory [29–31] and well justified for small wave amplitudes [32] and the background magnetic field inhomogeneity [33]. The important generalization of this approach for large amplitude waves can be performed under assumption of a broad wave spectrum (i.e., a large wave ensemble) [e.g., 34, 35], for which the effects of nonlinear trapping and phase bunching are essentially reduced to particle diffusion due to nonlinear resonance destruction. For systems with well separated in space and time large amplitude wave packets the nonlinear trapping and phase bunching result in significantly nondiffusive evolution of resonant particle ensemble. Therefore, the inclusion of large amplitude waves into diffusion approach should consist in development of additional operators acting on distribution function and describing nonlinear resonant interac-

tion.

Unlike the diffusion by small amplitude waves, the nonlinear resonant interaction can result in significant change of charged particle characteristics (e.g., energy) within a single resonance. This is effect of phase trapping, when wave intensity is sufficiently high to trap particles and transport them at long distances in the phase space. Such trappings cannot be described by differential operators (due to large change of particle characteristics), and nonlocal integral operators should be used. In case of periodic harmonic waves, such operators can be derived using the Hamiltonian theory of the resonant interaction [36] or numerically [37, 38]. The corresponding kinetic equation describes particle rapid transport in the phase space (driven by trapping) and drift (driven by scattering). The competition of these processes results in evolution of the particle velocity distribution [38–40]. However, many assumptions and simplifications used to derive this generalized Fokker-Planck equation cannot be applied for systems with non-harmonic waves, when the efficiency of the resonant interaction depends on the position of the resonant wave within the localized wave-packet. Previous analytical investigations of such operator derived for electrostatic [39] and electromagnetic [40] waves were based on equations derived for infinite plane monohromanic waves [36], and the important effect of the wave localization (wave propagation in form of wave-packets) was not studied theoretically.

This paper is focused on the theoretical model describing the nonlinear resonance of charged particles and localized wave-packets. We consider a system where Landau-resonant electrons interact with large amplitude wave-packets propagating in an inhomogeneous magnetic field and carrying the field-aligned electric fields. We also consider the effect of the wave-packet evolution, when the group velocity of the packet propagation differs from the phase velocity of propagation of waves within this packet. We use the equations of electron motion to describe systems with resonant electrons and electrostatic solitons [41, 42], or localized pulses of the field-aligned electric field carried by kinetic Alfven waves [43–45]. Moreover, the same approach can be applied to plasma systems with electromagnetic waves [e.g., see an example in 38, 46]. Although we consider a quite general plasma system (electron resonant interaction with the intense field-aligned electric fields propagating in the form of wave-packets), which is similar to the problem of electron resonant acceleration by Langmuir waves in inertial confinement fusion experiments [e.g., 47–49], we do not take into account many effects (e.g., resonant particle feedback to waves) important for accurate modeling of such systems. Therefore, our study mostly describes a new approach for resonant wave-particle consideration (with some applications to the geophysical systems, see Discussion), but further investigations are required to expand the approach on the laboratory plasma systems.

Paper is organized as follows: section II describes main system equations, section III describes the equations for resonant interaction and explains the role of a wave-packet evolution in the resonant particle acceleration, section IV introduces the integral operator acting on the particle distribution function and tests the basic properties of this operator, section V provides the solution of the kinetic equation with the derived operator, and section VII contains discussion of obtained results.

II. MAIN EQUATIONS

We consider Landau resonance of nonrelativistic charged particles (mass m, charge $-e$) moving in the inhomogeneous background magnetic field $\mathbf{B}$ with an electromagnetic wave defined by vector and scalar potentials, $\tilde{\mathbf{A}}$ and $\tilde{\varphi}$. The wave energy is assumed to be much smaller than the particle kinetic energy, and thus the Hamiltonian takes the form

$$H = \frac{1}{2m}\left(\mathbf{p} + \frac{e}{c}\mathbf{A}_0\right)^2 + \frac{e}{mc}\left(\mathbf{p} + \frac{e}{c}\mathbf{A}_0\right)\tilde{\mathbf{A}} - e\tilde{\varphi} \quad (1)$$

where $\mathbf{p}$ is the generalized momentum conjugated to the coordinate $\mathbf{r}$, $\mathbf{A}_0$ is the vector potential corresponding to the background magnetic field. The wave-fields, $\tilde{\mathbf{A}}$ and $\tilde{\varphi}$, can be presented as a multiplication of periodical functions of wave phase ϕ (such that $\nabla\phi = \mathbf{K}$ is the wave vector and $\dot{\phi} = -\omega$ is the wave frequency) and functions smoothly depending on spatial coordinates and time. In a sufficiently strong background magnetic field, the gyrorotation is the fastest type of motion. Thus, we can introduce the magnetic moment μ (ratio of the particle energy component transverse to the magnetic field and magnetic field magnitude) as a new variable [see, e.g., 50] and expand the wave fields into the series of gyroharmonics [see, e.g., 51, 52]:

$$H = \frac{1}{2m}p_\parallel^2 + \mu B + \sum_n W_n\left(\mu, p_\parallel, s\right)\sin\phi_n \quad (2)$$

where $\dot{\phi}_n = k\dot{s} + neB/mc - \omega$, k is the field-aligned component of the wave vector and field-aligned coordinate, $(s, p_\parallel)$ are the field-aligned coordinate and generalized momentum., eB/mc is the gyrofequency. In sufficiently strong background field (i.e., sufficiently large eB/mc) resonances with different numbers n do not overlap [see details in, e.g., 53] and each term of the sum $\sum_n$ can be considered separately. The Landau resonance corresponds to $n = 0$, when ϕ_n does not depend on the gyrophase. Therefore, $\dot{\mu} = 0$ and μ is the invariant of motion [50, 54]. For this resonance, Hamiltonian (2) can be rewritten as

$$H = \frac{1}{2m}p_\parallel^2 + \mu B + W_0\left(p_\parallel, s\right)\sin\phi(s,t) \quad (3)$$

where $\mu = const$. Hamiltonian (3) describes the electron resonant interaction with electromagnetic waves through the Landau resonance. For purely electrostatic waves W_0 does not depend on $p_\parallel$ and the term $W_0\sin\phi$ equals to

the wave potential $-e\Phi(s,t)$. For electromagnetic waves, W_0 can depend on $p_\parallel$ [see, e.g., 40, 51, 52]. For simplicity we omit this W_0 dependence in further consideration but note that the general conclusions do not depend on a particular form of W_0. Therefore, we consider Hamiltonian

$$H_0 = \frac{1}{2m}p_\parallel^2 + \mu B\left(s\right) - e\Phi\left(s,t\right) \tag{4}$$

We introduce dimensionless coordinates $z = s/R$, $p = p_\parallel/\sqrt{h_0 m}$, parameter $\Omega_b^2 = \mu B(0)/h$, field $b = B/B(0)$, time $t \to t\sqrt{h_0/m}/R$, and wave potential amplitude $\varepsilon = -e\Phi_0/h_0$, where h_0 is a typical particle energy, R is a spatial scale of B variation, and $\Phi = \Phi_0 u(z) f(z,t)$. Function $u(z)$ describes the distribution of the wave intensity along magnetic field lines, and function $f(z,t)$ defines the shape of wave-packets. New Hamiltonian $H = H_0/h_0$ takes the form

$$H = \frac{1}{2}p^2 + \Omega_b^2 b\left(z\right) + \varepsilon u\left(z\right) f\left(z,t\right) \tag{5}$$

For $\Omega_b \to 0$ (i.e., for a very weak background magnetic field or almost field-aligned charged particles) this Hamiltonian system was considered in [55].

To set function f, we consider a localized wave-packet propagating with a phase velocity v_ϕ and a different group velocity v_g. Following [56, 57] we introduce the effect of $v_\phi \neq v_g$ as a difference of velocities of wave and envelope motions:

$$\begin{aligned} &f\left(z,t\right) = \exp\left(-q\psi^2\right)\sin\left(\phi\right) \\ &\phi = k\left(z - v_\phi t\right) + \phi_0 \\ &\psi = k\left(z - v_g t\right) + \psi_0 = \varphi_0 + \phi + \Omega t \end{aligned} \tag{6}$$

where k is a wavenumber, ϕ_0 and ψ_0 are initial phases, $\Omega = k(v_\phi - v_g) \ll k v_\phi$ (i.e., we consider a small difference $|v_\phi - v_g| \ll v_\phi$), and $\varphi_0 = \psi_0 - \phi_0$. Parameter $q = (2\pi N)^{-2}$ determines a number of wavelengths N within one wave-packet. For wave characteristics we use the same normalization as for particle coordinates, but keep the notations: $k \to kR$, $(v_\phi, v_g) \to (v_\phi, v_g)/\sqrt{h_0/m}$.

For investigation of system (5, 6), we fix $\Omega_b = 1$, use magnetic field model with $b(z) = 1 + z^2/2 + b_0 z^4/4$ [see discussion why $b_0 \neq 0$ is needed for investigation of nonlinear resonant interaction in 39], and consider $u = 0$ for $z < 0$ and $u = (u_0(z) - u_0(0))/2$ for $z > 0$, $u_0(z) = 1 + \tanh((z-1)/3)$. This distribution of the wave intensity imitates the wave generation at $z = 0$ and propagation along magnetic field lines. Zero u for $z < 0$ is taken for simplicity, i.e. particles oscillating in potential $\Omega_b^2 b(z)$ interact with waves only once per period of oscillations. Wavelength is assumed to be much shorter than R, whereas wave potential amplitude is much smaller than the particle energy: $k \gg 1$ and $\varepsilon \ll 1$. This a typical situation for, e.g., electrostatic and electromagnetic waves propagating in the Earth radiation belts (see Discussion for details).

Figure 1 shows three examples of particle trajectories obtained from the numerical integration of Hamiltonian equations of motion for system (5). In the absence of a wave the particle oscillates in $\Omega_b^2 b(z)$ potential and it's z, p coordinates change periodically (see Fig. 1(a)). In the presence of the wave, the particle can pass through the resonance $\dot{\phi} = 0$ (stationary wave point), determined as: $\dot{z} = \partial H/\partial p = p = v_\phi$. Resonance crossing results in particle scattering (small change of the particle energy) and particle trapping characterized by a long particle motion with the wave ($p = v_\phi$, see Fig. 1(b)). For harmonic wave with $N \to \infty$ the resonance trapping does not depend on characteristics of the initial particle position in (z,p) trajectory. All particles with the same energy are trapped at the same z_{trap} and escape from the resonance at almost the same z_{esc} (detrapping). Trapped particle motion results in energy gain $\Delta h = \Omega_b^2(b(z_{esc}) - b(z_{trap}))$ ($p = v_\phi$ does not change in the resonance), and thus all trapped particles gain the same energy (see Fig. 1(b)). Situation changes for a finite wave-packet (finite N), when particles trapped into different waves (different wave periods within wave-packet) gain different energy (see Fig. 1(c)). Situation even more complicates for a wave-packet propagating with velocity v_g different from wave phase velocity v_ϕ. In this case, the trapped particle can travel along wave-packet and the energy gain depends significantly on wave parameters (wave phase) at the moment of trapping (see Fig. 1(d)). Taking apart the scattering process, we focus in this paper on properties of particle trapping and dependence of these properties on system parameters: N and $\Omega = k(v_\phi - v_g)$.

III. RESONANT TRAPPING: EFFECTS OF WAVE-PACKET EVOLUTION

To consider effects of a finite wave-packet and $\Omega \neq 0$ on the resonant wave-particle interaction, we follow the standard procedure [58, 59] and investigate Hamiltonian (5) around the resonance $\dot{\phi} = 0$. First, we use the generating function $W_1 = k(z - v_\phi t)I_\phi + P_z z$ to introduce new variable $\phi = k(z - v_\phi t)$ and conjugated momentum I_ϕ. New momentum P_z and Hamiltonian $\mathcal{F}$ have the form $P_z = p - kI_\phi$ and

$$\mathcal{F} = -kv_\phi I_\phi + \frac{1}{2}\left(P_z + kI_\phi\right)^2 + \Omega_b^2 b\left(z\right) + \varepsilon u\left(z\right) f\left(\phi,\tau\right) \tag{7}$$

where $\tau = \Omega t$ and new z coordinate equals to the old coordinate. The resonant condition $\partial\mathcal{F}/\partial I_\phi = 0$ written through variables I_ϕ, P_z gives the equation for resonant $I_\phi = I_R$:

$$I_R = \left(v_\phi - P_z\right)/k \tag{8}$$

We expand Hamiltonian $\mathcal{F}$ around $I_\phi = I_R$:

$$\mathcal{F} = v_\phi P_z - \frac{1}{2}v_\phi^2 + \frac{1}{2}k^2\left(I_\phi - I_R\right)^2 + \Omega_b^2 b\left(z\right) + \varepsilon u\left(z\right) f\left(\phi,\tau\right) \tag{9}$$

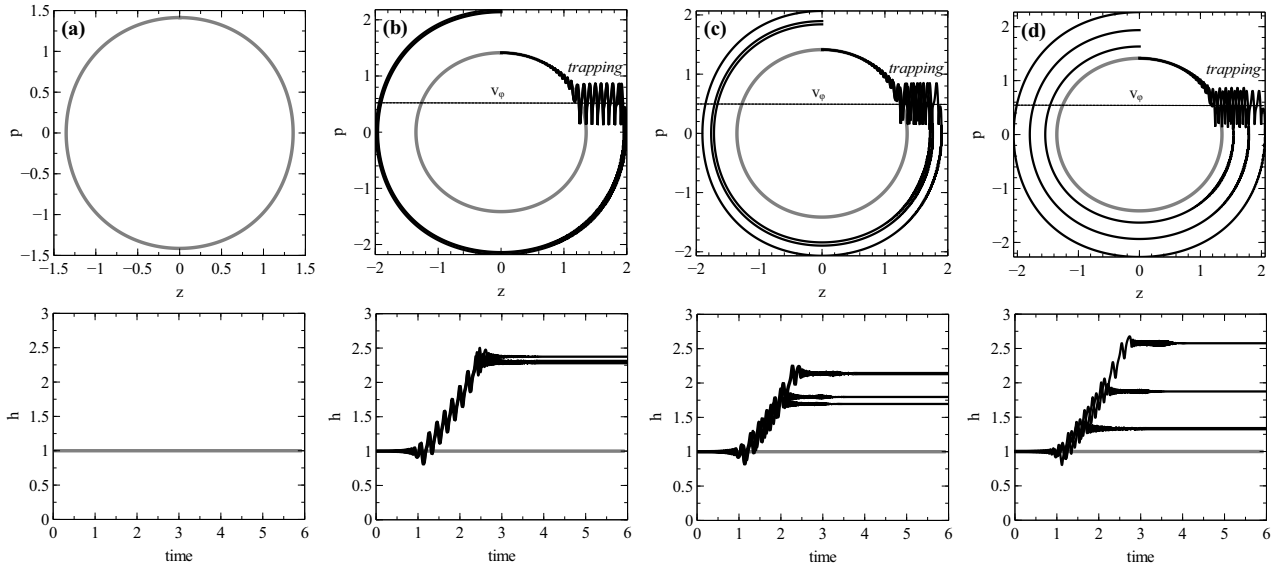

FIG. 1: Particle trajectories: top panels show trajectories in the (z, p) plane, and bottom panels show the evolution of the particle energy h for one resonant interaction (we select trajectories of trapped particles). Wave characteristics are: (a) $\varepsilon = 0$, (b) $N \to \infty$, $\Omega = 0$ and $\varepsilon = 0.05$, (c) $N = 25$, $\Omega = 0$ and $\varepsilon = 0.05$, (d) $N = 25$, $\Omega/k = 0.1$ and $\varepsilon = 0.05$. System parameters are: $\Omega_b = 1$, $v_\phi = 0.5$, $k = 250$, $\tilde{b}_0 = 2h_0 b_0/\Omega_b^2 = 0.1$.

Using the generating function $W_2 = (I_\phi - I_R)\phi + Pz$ we introduce new variables $K = I_\phi - I_R$, $P = P_z$, $Z = z + \phi(\partial I_R/\partial P_z) = z - \phi/k$. The corresponding Hamiltonian can be presented as

$$\tilde{\mathcal{F}} = v_\phi P - \frac{1}{2}v_\phi^2 + \Omega_b^2 b\,(Z + \phi/k) + \frac{1}{2}k^2K^2 + \varepsilon u\,(Z + \phi/k)\,f\,(\phi, \tau) \qquad (10)$$

Expanding over ϕ/k, we obtain $\tilde{\mathcal{F}} = \Lambda(Z, P) + H_\phi(K, \phi, Z)$:

$$\Lambda = -\frac{1}{2}v_\phi^2 + v_\phi P + \Omega_b^2 b\,(Z)\,, \qquad (11)$$
$$H_\phi = \frac{1}{2}k^2K^2 + \Omega_b^2\frac{\partial b}{\partial Z}\frac{\phi}{k} + \varepsilon u\,(Z)\,f\,(\phi, \tau)$$

where variables (Z, P) change slowly, and variables (ϕ, K) change fast ($\dot{\phi} = k^2K$ and $k \gg 1$). Hamiltonian H_ϕ describes particle motion in the resonance, whereas parameters of Hamiltonian H_ϕ depend on Z coordinate described by Hamiltonian Λ. For fixed Z and slow time τ ($\Omega \ll k$), phase portrait of Hamiltonian H_ϕ is shown in Fig. 2(a). This portrait contains many loops with closed trajectories inside. Particles moving along these closed trajectories are oscillating around the resonance $K = 0$ and move with the wave, i.e. these are trapped particles. For $\Omega = 0$ ($\tau = 0$), the phase portrait varies only with Z, i.e. varies along the resonant trajectory. This allows particles moving along open trajectories become trapped, i.e. such particles cross the separatrix demarcating regions with open and closed trajectories. Trapped particles move with the wave ($\dot{Z} = \partial\Lambda/\partial P = v_\phi$, and their energy increases as $\sim \Omega_b^2 b(Z)$). At some Z, term $\sim \partial b/\partial Z$ in H_ϕ becomes sufficiently large to exclude all closed loops from the phase portrait (see Fig. 2(b, c)).

Situation is more complicated when the wave-packet evolves with time ($\Omega \neq 0$). In this case, the phase portrait changes both with Z and τ. Figures 2(d,e,f) shows three states of the phase portrait with initial state from Fig. 2(a) (when $Z = Z_0$ and $\varphi_0 = 0$), and $\tau = \varphi_0/\Omega + \Omega(Z - Z_0)/v_\phi$. Despite Z increases, the areas surrounded by some closed loops are growing (due to time evolution of the wave-packet) before eventually decrease to zero. This effect explains why in the system with $\Omega \neq 0$ trapped particles can stay in the resonance longer and gain more energy (see test trajectories in Fig. 1).

The coordinate of a particle trapping into the resonance, Z_{trap} (note, Z for system (11) coincides with z for system (5)) can be defined from the combination of the resonant condition ($I = I_R$, i.e., $P = P_z = v_\phi$) and conservation of the total energy for Hamiltonian $\mathcal{F}$ ($\partial\mathcal{F}/\partial t = 0$): $b(Z_{trap}) = (h - v_\phi^2/2)/\Omega_b^2$ where h is an initial particle energy in Hamiltonian (5). Position where the particle escapes from the resonance, Z_{esc}, is defined by the simple relation: the area surrounded by the separatrix in the phase portrait shown in Fig. 2 should be the same in the moments of trapping and escaping from the resonance [see, e.g., 58, 59]. To define Z_{esc} we write the equation for area surrounded by the separatrix:

$$S = \oint K d\phi = \frac{2\sqrt{2k\varepsilon u\,(Z)}}{k^{3/2}} \qquad (12)$$

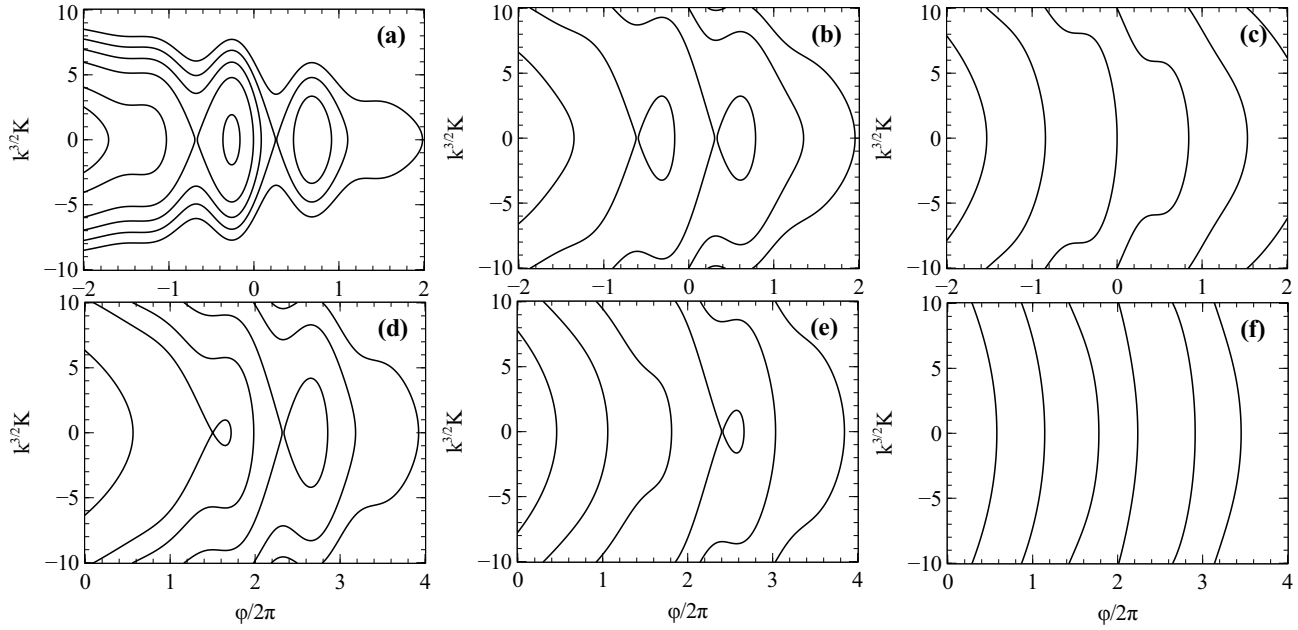

FIG. 2: Phase portraits for the system with $\Omega = 0$ (a, b, c) and for the system with $\Omega = 10/250$ (d, e, f). Panel (a): Z coordinate equals to the resonant value. Panel (b): Z is larger than the resonant value, but the separatrix loop still exists. Panel (c): Z is larger than the resonant value, and there is no separatrix loop. Panel (d): Z the same as in panel (b). Panel (e): Z the same as in panel (c), but the separatrix loop still exists. Panel (f): Z is larger than in panel (d), and there is no separatrix loop.

$$\times \int_{\phi_-}^{\phi_+} \sqrt{a\left(\phi_+ - \phi\right) + f\left(\phi_+, \tau\right) - f\left(\phi, \tau\right)}\, d\phi$$

where $a = \Omega_b^2(\partial b/\partial Z)/(k\varepsilon u(Z))$, ϕ_- is a root of equation $a = -df/d\phi$, whereas ϕ_+ is a root of equation $a\left(\phi_+ - \phi\right) + f\left(\phi_+, \tau\right) - f\left(\phi, \tau\right) = 0$ (for $a > 0$ ϕ_- is smaller than ϕ_+, and for $a < 0$ the direction of integration reverses). Area S depends both on Z and τ. Figure 3 shows three examples of $S(Z, \tau)$. For $\Omega = 0$ profile $S(Z, \tau)$ does not depend on τ, whereas for $\Omega \neq 0$ we have 2D surface $S(Z, \tau)$. Trajectories of trapped particles in this figure are shown by straight lines ($Z = tv_\phi + const = \tau v_\phi/\Omega + const$). For $\Omega = 0$, the escape coordinate Z_{esc} (coordinate of detrapping) does not depend on τ and is defined only by trapping position Z_{trap}, whereas for $\Omega \neq 0$ the position of escaping Z_{esc} depends on the moment when particles are trapped.

IV. OPERATOR OF NONLINEAR TRANSPORT

To characterize the energy change for particle ensemble we consider map $h_{final} = h_{final}(h, \varphi_0)$ describing final particle energy as a function of the initial energy h and initial wave phase φ_0. This map is constructed for a time interval of a single resonant interaction, i.e. for one period of slow particle oscillations in the (z, p) plane. During this interval, each particle (having some ϕ_0) crosses the resonant Z_{trap} once, and thus can interact with the wave-packet only once (or can skip the resonant interaction if φ_0 corresponds to absence of the resonance). Such resonant interaction results in energy change $h \to h_{final}$ that depends on h and φ_0. Figures 4(a,b,c) show h_{final} map plotting for fixed h and different φ_0. In the system with $\Omega = 0$ and $N \to \infty$, function $h_{final}(\varphi_0)$ is periodic with sharp maxima ($h_{final} > h$) and wider minima ($h_{final} < h$). These minima are due to particle scattering with a small energy decrease, whereas maxima are due to trapping and acceleration. Analysis of phase portraits and areas S shown in Figs.2, 3 provides main characteristics of this map: ratio of scales of φ_0 ranges related to acceleration and deceleration (so called probability of trapping, see [60]) and magnitude values (minimum and maximum) of h_{final} [see examples in 61–63]. Such characteristics can be used to construct the operator acting on the particle distribution $\Psi(h)$ and describing a long-term evolution of this distribution due to scattering and trapping (under assumption of the uniform distribution of φ_0 values, see [36, 39, 40]).

Systems with a finite N (even if $\Omega = 0$) provide significant difficulties for construction of such operator analytically. Indeed, Fig. 4(b) shows that for fixed h, map $h_{final}(\varphi_0)$ is not periodic, i.e. we still can separate each 2π-interval of φ_0 values to two ranges with $h_{final} < h$ and $h_{final} > h$, but magnitudes of h_{final} vary form one 2π-interval to another interval. Situation becomes even more complicated for systems with $\Omega \neq 0$, where map $h_{final}(\varphi_0)$ loses the symmetry relative to the center, see

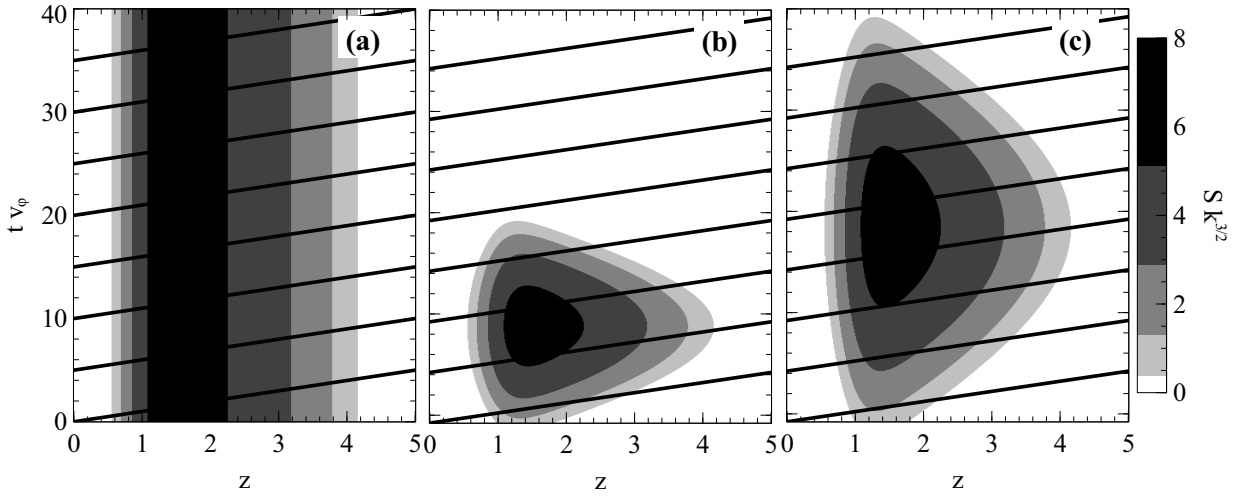

FIG. 3: Areas surrounded by the separatrix loop for (a) $\Omega/k = 0$, (b) $\Omega/k = 10/250$, (c) $\Omega/k = 5/250$. Lines show resonant trajectories.

Fig. 4(c).

The range of φ_0 shown in Fig. 4 can be considered as a time interval $\Delta\varphi_0/k = v_\phi \Delta t$ during which the wave-packet passes through the system, i.e. time interval between the first resonant interaction of particles with waves within this wave-packet and the last resonant interaction. This interval is longer than one period of particle oscillations in (z, p) plane, and thus many particles experience several resonant interaction during this interval. As a result, the construction of analytical operator acting on distribution $\Psi(h)$ becomes very complicated problem requiring calculation of trapping probabilities and amplitudes of acceleration/deceleration for each 2π-interval of φ_0 and following combination of these information.

In periodical system with $N \to \infty$, $\Omega = 0$ (where one needs to define all characteristics of the resonant interaction only for one 2π-period of φ_0 values), the unit time interval is the interval between two resonant interactions, i.e. the period of oscillations in (z, p) plane. For systems with a finite N we can consider a longer unit time interval including the entire φ_0 range shown in Fig. 4(b,c). Thus, we can construct probability distribution $\mathcal{P}(h_{final}, h)$ showing the probability for particles with the initial energy h to have final energy within the range $[h_{final}, h_{final} + \Delta h_{final}]$ after the wave-packet passage through the system.

To test this approach, we start with a simple single-resonance operator, i.e. we consider $\mathcal{P}(h_{final}, h)$ that describes energy change due to one resonant interaction of particles and wave-packet (see Fig. 4). We take $N \to \infty$, set a net in h-space, and for each initial h consider 10^4 particles distributed uniformly along the trajectory in (z, p) space. Particle trajectories are integrated numerically until the first resonant interaction, and then particles are distributed in the h_{final}-space. Figure 5(a) shows the final probability distribution $\mathcal{P}(h_{final}, h)$ (note that $\int_0^\infty \mathcal{P}(h_{final}, h) dh_{final} = 1$). There are two distinct particle populations in this distribution: decelerated (scattered) particles with $h_{final} < h$ and accelerated (trapped) particles with $h_{final} > h$. To check the obtained distribution, we take into account properties of

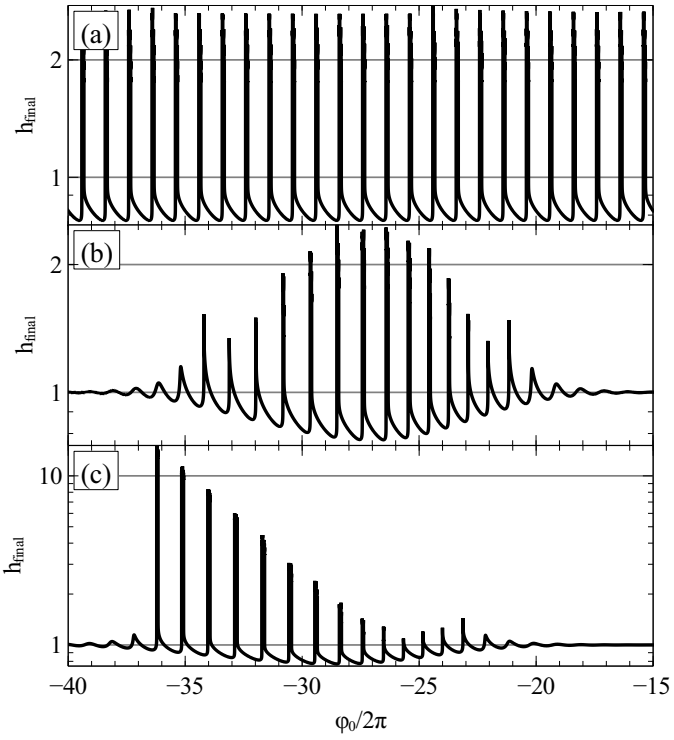

FIG. 4: The final energy after a single resonant interaction as a function of the initial wave phase : (a) $N \to \infty$ and $\Omega/k = 0$, (b) $N = 25$ and $\Omega/k = 0$, (c) $N = 25$ and $\Omega/k = 10/250$. The initial energy equals to one.

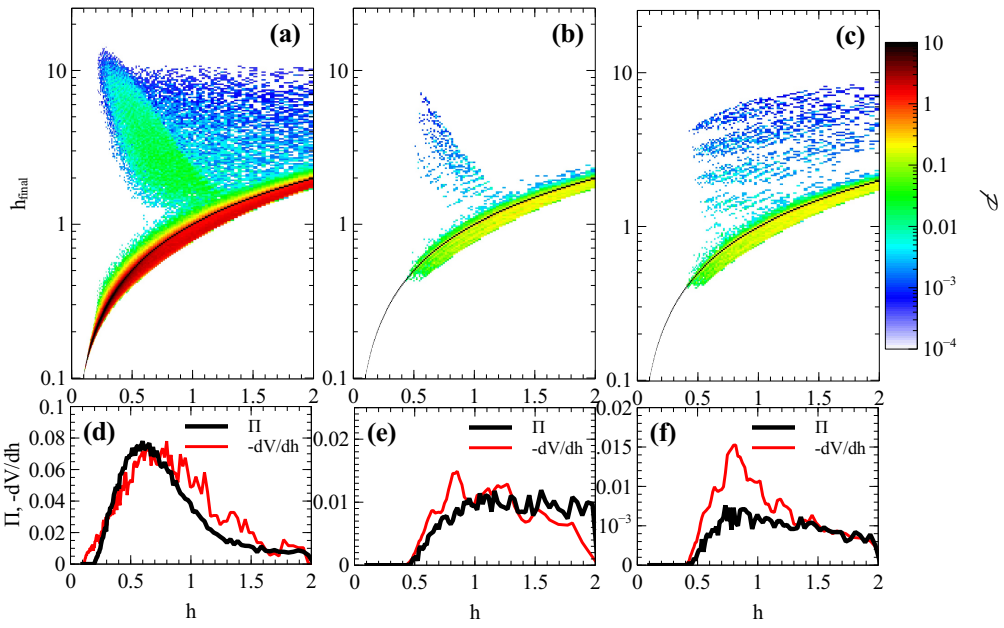

FIG. 5: Top panels show distributions $\mathcal{P}(h_{final}, h)$ for a single resonant interaction (system contains one wave-packet and particles are traced during a quarter of the bounce period): (a) $N \to \infty$ and $\Omega/k = 0$, (b) $N = 5$ and $\Omega/k = 0$, (c) $N = 5$ and $\Omega/k = 10/250$. Black curve shows $h_{final} = h$. Bottom panels show the integral properties of these distributions (see Eqs. (13, 14)).

the nonlinear wave-particle interaction. We calculate the total probability of particles with the initial energy h to be trapped

$$\Pi(h) = \int\limits_{h<h_{final}} \mathcal{P}(h, h_{final}) dh_{final} \qquad (13)$$

and the total energy change for scattered particles

$$V(h) = \int\limits_{h>h_{final}} (h_{final} - h)\, \mathcal{P}(h, h_{final}) dh_{final} \qquad (14)$$

Integration of $\mathcal{P}(h_{final}, h)$ over initial energies $h < h_{final}$ gives the total probability of particles to have energy h due to trapping, whereas integration $(h_{final} - h)\mathcal{P}(h_{final}, h)$ over initial energies $h > h_{final}$ gives the average particle energy change due to scattering. For an individual resonant interaction with periodical wave, Π and V are connected to each other by a simple relation which can be derived from the consideration of the resonant phase fluxes [see 36, 60]: $\Pi = -dV/dh$ (note this relation connects the probability of trapping (relative number of trapped particles) and average change of scattered particle energy; for systems with constant period between two resonant interactions V equals (with some constant factor) to the scattering particle drift velocity [e.g., 36]). Figure 5(d) shows Π and $-dV/dh$ calculated from Eqs. (13,14) for $\mathcal{P}(h_{final}, h)$ shown in Fig. 5(a). Numerically obtained Π and $-dV/dh$ are very close to each other, thus we confirm that the approach with $\mathcal{P}(h_{final}, h)$ construction works well.

Relation $\Pi = -dV/dh$ works even for the localized wave-packet. Figure 5(b) shows the corresponding operator $\mathcal{P}(h_{final}, h)$ for $N = 5$ and $\Omega = 0$, whereas Π and V calculated for this probability distribution are shown in Fig. 5(e). This distribution is calculated for a single resonant interaction, but unlike the harmonic wave ($N \to \infty$, see Figs. 5(a,d)), less particles can be efficiently accelerated by a localized wave-packet, and the corresponding probability of trapping is smaller. The evolution of wave-packet ($\Omega \neq 0$) makes system more complicated, and the relation $\Pi = -dV/dh$ does not work for small energies anymore (see Figs.5(c,f)).

Probability distributions shown in Fig. 5 are plotted for a short time interval including only one resonant interaction. However, we can construct a similar distribution for the time interval sufficiently long to allow a localized wave-packet pass through the system. During this interval, some particles make several bounce rotations (cross Z_{trap} several times) and can resonate with wave-packets several times, i.e. these particle experience several $h \to h_{final}$ energy changes. We distribute 10^4 particles uniformly along trajectory in (z, p) space and integrate their trajectories numerically for time interval needed to particle to pass ϕ range slightly exceeding φ_0 range from Fig. 4. Figure 6 shows the final probability distributions for three different systems. Similar to Fig. 5, there are decelerated (scattered) particles with $h_{final} < h$ and accelerated (trapped) particles with $h_{final} > h$. Accelerated particles form several local maxima of $\mathcal{P}$, and each maximum corresponds to the resonant interaction with one particular wave from the wave-packet. Different wave

amplitudes and different evolution of these amplitudes due to $\sim \exp(-q\psi^2)$ provide different h_{final}. Unlike the distributions constructed for a single resonant interaction (see Fig. 5), distributions including several interactions do not demonstrate the relation $\Pi = -dV/dh$ for the entire range of initial energies. Figures 6(d,e,f) show that only for large initial energies we have $\Pi = -dV/dh$, whereas for $h < 0.5$ the drift velocity has stronger gradients changing sign around the peak value of Π. This can be an effect of the combination of trapping and scattering for particles contributing to V calculated using Eq. (14).

V. KINETIC EQUATIONS

The probability distribution $\mathcal{P}(h_{final}, h)$ shown in Fig. 6 can be used to calculate the evolution of the particle distribution $\Psi(h,t)$. We write the master equation [64] describing the relation between $\Psi(h, t+\Delta t)$ and $\Psi(h,t)$, where Δt is a time interval needed for one wave packet to pass through the system:

$$\Psi\left(h, t+\Delta t\right) = \int_0^\infty \Psi\left(\tilde{h}, t\right) \mathcal{P}\left(\tilde{h}, h\right) d\tilde{h} \qquad (15)$$

Figure 7 shows three examples of solutions of Eq. (15) for $\mathcal{P}$ from Fig. 6. In case on non-evolving wave-packet ($\Omega = 0$, Fig. 7(d)), the distribution function Ψ changes with time as follows: the high-energy part of Ψ increases due to particle trapping and acceleration, for intermediate energies Ψ decreases due to particle drift with energy loss, and for very small energies Ψ increases because particles arriving to this region due to drift cannot be trapped due to the very small wave amplitude (corresponding resonant z is small and $u(z)$ tends to zero). This evolution is determined by the wave amplitude distribution. Note also that the operator $\mathcal{P}$ may describe diffusion insufficiently accurately, because energy change due to diffusion is so small that initial and final energies both fall into the same energy bin in the h-net. Diffusion is playing an important role in the systems where low-amplitude wave signals are almost continuously present. However, it is expected to be much less important in case of separate intense wave packets when the number of considered resonant interactions is small.

The evolution of the wave-packet ($\Omega \neq 0$) results in a more complicated structure of $\Psi(h,t)$ (compare Fig.7(d) and Fig.7(e,f)). For moderate Ω, each wave-period within the wave-packet provides acceleration of trapped particles up to some energy (see Fig. 7(c)). This results in a quasi-periodical structure of $\Psi(h)$ in the high energy range. The wave-packet evolution leads to variation of wave-amplitude at the scale of a wave-period in this packet. Thus, some waves can transport trapped particles for a longer time than other waves and provide more effective acceleration. This effect resembles the formation of a quasi-periodical energy distribution of trapped particles in a system where particles can spend more or less time in the resonance with waves depending on the initial wave phase [see 65]. The evolution at intermediate and low energy ranges are similar for all cases shown in Fig. 7, i.e. scattering is only weakly perturbed by the wave-packet evolution.

To check the applicability of Eq. (15) and the accuracy of the constructed operator $\sim \mathcal{P}$, we compare solutions of this equation with results of numerical integration of 10^6 trajectories within the time interval including many wave-packets. Figure 8 shows such a comparison for two Ω values and two initial distributions $\Psi_{t=0}$. Numerical solutions coincide well with solutions of Eq. (15), confirming the correctness of our approach.

VI. Ω/k DISTRIBUTION

In more realistic systems, wave-packets do not have the same Ω/k parameter, but rather have some distribution $\mathrm{X}(\Omega/k)$. Therefore, to reproduce the evolution of the charged particle distribution in such systems, we need to construct $\mathcal{P}$ operators for a set of Ω/k and then average these operators as

$$\mathrm{P} = \sum_i \mathcal{P}\left(\varpi_i\right) \mathrm{X}\left(\varpi_i\right), \quad \varpi = \Omega/k \qquad (16)$$

Figure 9 shows three examples of such averaged operators P. Independently of the particular profile of the X distribution, the averaged P has the same boundaries in the (h_{final}, h) space (different X correspond to different P values within these boundaries). These boundaries are defined by the $h_{final}(h, \varphi_0)$ function, which can be evaluated analytically for each Ω/k value.

To reproduce the shape of the P operator from Fig. 9, we first find $\max\left(h_{final}(h,\varphi_0)\right)$ for φ_0 covering the entire range of the initial phases allowing the resonant interaction. This procedure provides $\max\left(h_{final}\right)$ as a function of initial energy, h, and the wave-packet characteristic Ω/k. For different Ω/k, we plot $\max\left(h_{final}(h)\right)$ together with one P operator in Fig. 10(a). Analytical boundaries well describe the shape of P, but we also need to evaluate P values within these boundaries. For this reason, we use the analytical equation $\Pi = -dV/dh$ with $V = v_\phi S/2\pi$ [36, 60] (area S is given by Eq. (12)). The probability of scattering is equal to $1-\Pi$ and corresponds to the final energy $h_{final} = h + V(h)$ (note $V < 0$). We evaluate Π, $1-\Pi$ for each bin in the (h, h_{final}) space with fixed φ_0 and Ω/k. Then, analytical probabilities $\Pi(\varphi_0, \Omega/k)$ are averaged over the uniform φ_0 distribution. Finally, we re-normalize the obtained analytical operator $\mathcal{P}$ to get $\int_0^\infty P(h_{final}, h) dh_{final} = 1$ and average it over the $\mathrm{X}(\Omega/k)$ distribution. Figure 10(b) shows such an analytically derived P operator for the uniform $\mathrm{X}(\Omega/k)$. Comparison of P from Fig. 9 and 10(b) shows that the analytical equations reproduce the main features of the distribution of the probability of trapping and scattering, but, of course, can miss some details related to the fine

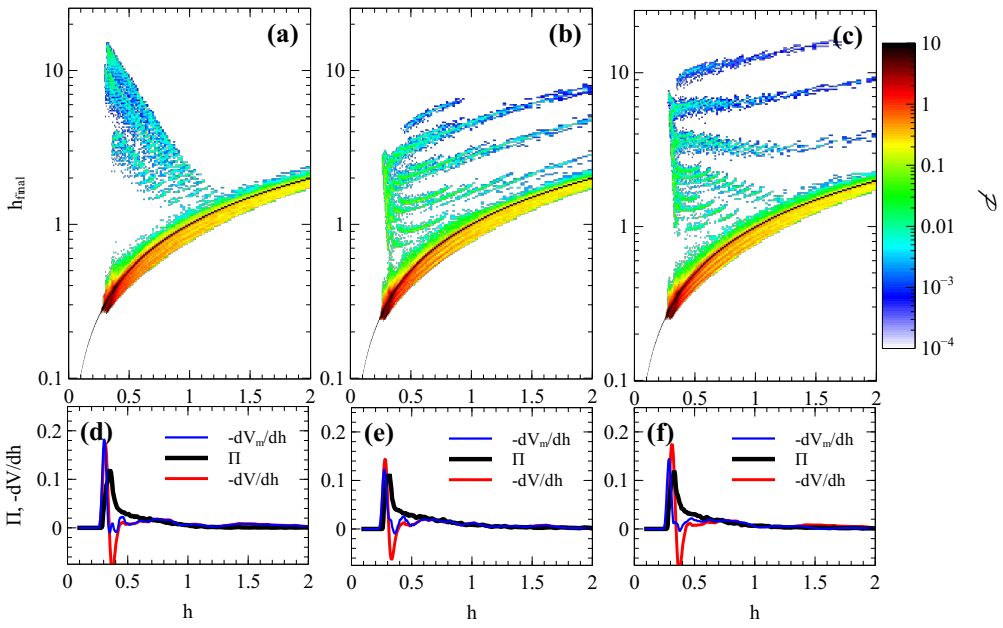

FIG. 6: Top panels show distributions $\mathcal{P}(h_{final}, h)$ for a time interval of one wave-packet passing through the system (the system contains one wave-packet and particles are traced during the interval of packet motion between $z = 0$ and $z = 5$ where $u \to 0$): (a) $N = 5$ and $\Omega/k = 0$, (b) $N = 5$ and $\Omega/k = 10/250$, (c) $N = 5$ and $\Omega/k = 5/250$. Black curve shows $h_{final} = h$. Bottom panels show integral properties of these distributions (see Eqs. (13, 14)). Blue curves show derivatives of modified drift velocity V_m, which is evaluated taking into account that during several resonant interactions some scattered particles become trapped and the final number of scattered particles ($h < h_{init}$) is lower than expected for one resonant interaction. This reduction of particles with $h < h_{init}$ corresponds to the multiplication factor $V_m = V/(1 + \ell)$ with $\ell = M^{-1} \sum_{n=1}^{M} \Pi(M - n)/(1 - M\Pi) = (1/2)\Pi(M - 1)/(1 - M\Pi)$ where M is the number of resonant interactions for the considered time interval ($M = 5$ is used to plot blue curves).

structure of the wave-particle interaction. Therefore, averaging over Ω/k results in some more universal shape of the probabilistic operator in the (h_{final}, h) plane (in comparison with $\mathcal{P}$ plotted for fixed Ω/k, see Figs. 6, 7), and this averaged operator P can be fitted by analytical equations. Neverheless, the accuracy of such an analytical description should be examined for each particular plasma system separately.

VII. DISCUSSION AND CONCLUSIONS

Figures 6(d-f) show an interesting property of the constructed operator $\sim \mathcal{P}(h_{final}, h)$: this operator satisfies the analytical equation $\Pi = -dV/dh$ in the high energy range, but it does not follow this relation at lower energies where dV/dh reverses. Deviations from the equation $\Pi = -dV/dh$ can be provided by two facts: the variation of the area (12) with time (equation $\Pi = -dV/dh$ was derived for $S = S(h)$ when $dS/dt = (dS/dh)(dh/dt)$, see [36]), and an interference of effects of several resonant interactions during the passage of one wave-packet through the system. Indeed, Fig. 5(f) suggests that the direct dependence of S on time can result in violation of $\Pi = -dV/dh$, however, it does not lead to dV/dh reversal. Therefore, this reversal should be due to several resonant interactions when particles expected to be scattered and to lose their energy actually become trapped and evacuated from the domain $h_{final} < h$. Such an interference effect of trapping and scattering can hardly be included into an analytically constructed $\mathcal{P}$, and the proposed numerical approach for $\mathcal{P}$ construction represents a reasonable compromise between fully numerical simulations of the long term wave-particle interaction [e.g., 46, 66–68] and a fully analytical analysis of the $\mathcal{P}$ structure [e.g., 36, 40]. Moreover, averaging the system over a broad Ω/k distribution smooths many details of the $\mathcal{P}$ operator, and the resulting averaged operator P can then be described by the analytically derived P. Of course, such an averaging strongly depends on the system characteristics and the Ω/k distribution. Thus, the similarity of the numerically and analytically derived operators should be carefully examined for each particular plasma system separately.

Although this study deals with field-aligned wave fields, the resonant Hamiltonian (11) has a universal form and can be derived for other wave modes as well [e.g., 51, 52, 69, 70]. There are three main simplifications of initial system (5): small difference of phase and group wave velocities, a wave frequency constancy (for waves with weak dispersion and small chirping), and constant adiabatic invariant μ. If two first simplifications limit the

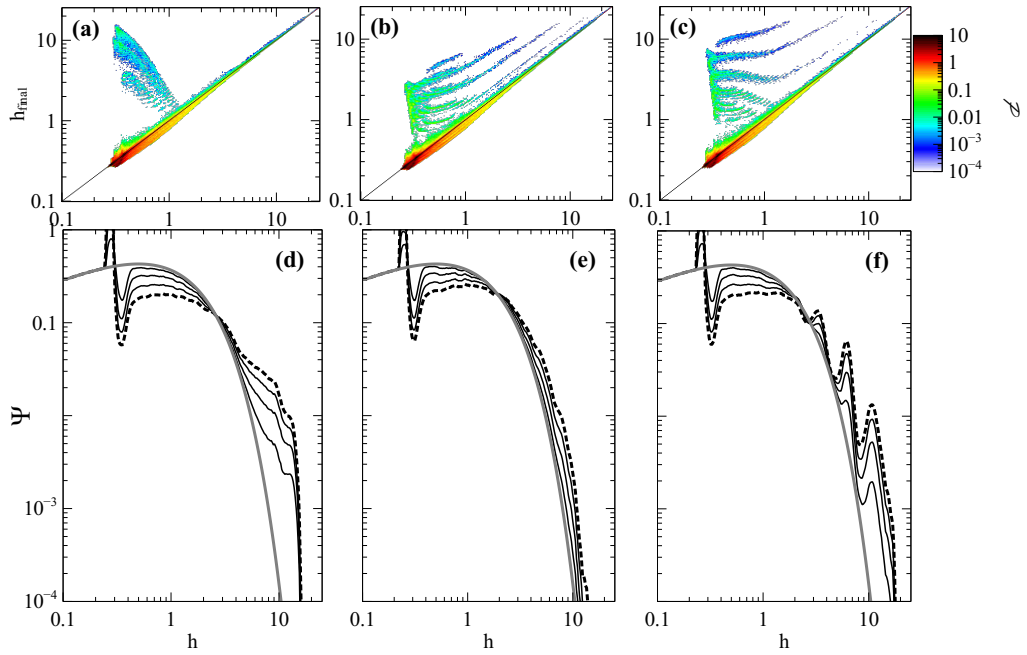

FIG. 7: Top panels show distributions $\mathcal{P}(h_{final}, h)$ for time interval of one wave-packet passing through the system: (a) $N = 5$ and $\Omega/k = 0$, (b) $N = 5$ and $\Omega/k = 10/250$, (c) $N = 5$ and $\Omega/k = 5/250$. Bottom panels show the evolution of particle distributions Ψ in these three systems. Grey line is for the initial distribution, dashed black line shows Ψ after interaction with 100 packets, solid black lines are for intermediate time moments. Numerical results are obtained in the system with periodical relaunching of wave-packets described by Eq. (6): when the peak (given by $\psi = 0$) of one packet launched from $z = 0$ (i.e., $\psi = 0$ for $z = 0$ at the launch time) reaches $z = 5$ (where $u \to 0$), a new packet is launched from $z = 0$ again. This procedure is repeated 100 times, i.e. there are 100 packets passing through the system.

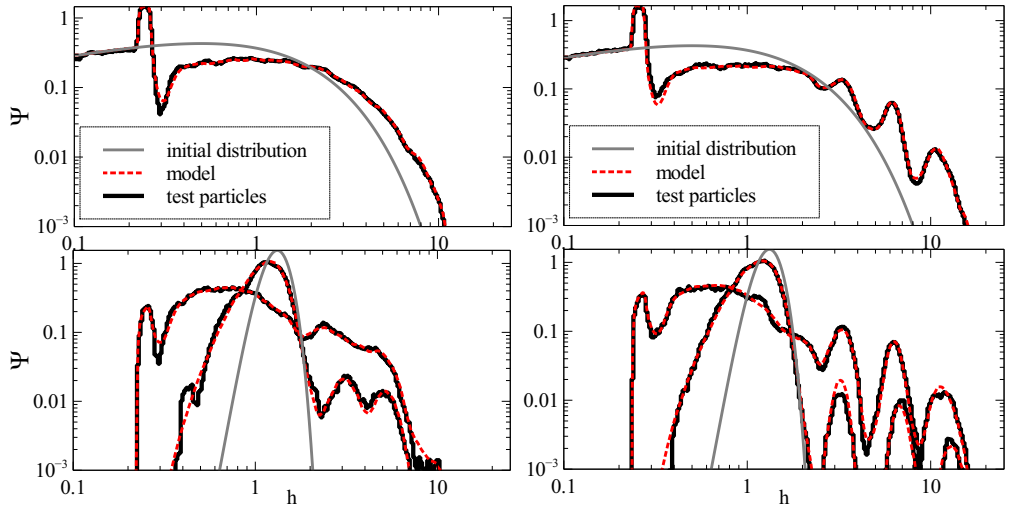

FIG. 8: Comparison of solutions of Eq. (15) and results of numerical integration of 10^6 trajectories for two systems: (a,c) $N = 5$ and $\Omega/k = 10/250$, (b,d) $N = 5$ and $\Omega/k = 5/250$. Grey line is for the initial distribution, black line shows test particle results, dashed red lines show solutions of Eq. (15). For top panels Ψ are shown for 100 interactions with wave-packets, for bottom panels Ψ are shown for 20 and for 100 interactions with wave-packets.

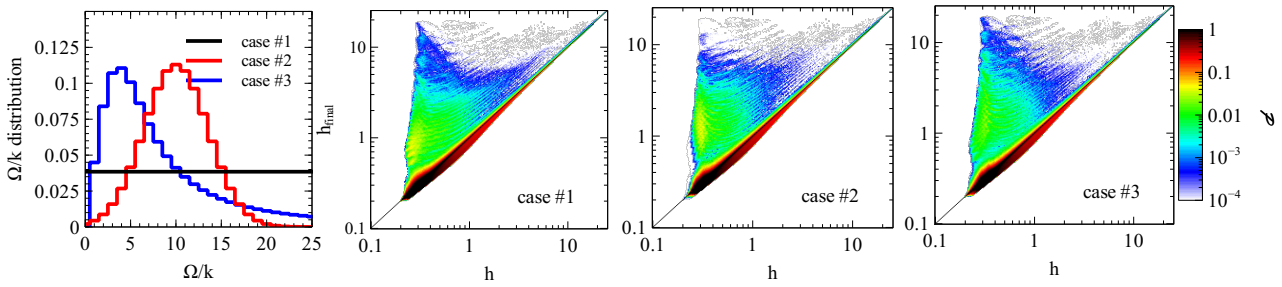

FIG. 9: Left panels shows three X(Ω/k) distributions, and three other panels show corresponding averaged operators P evaluated using Eq. (16).

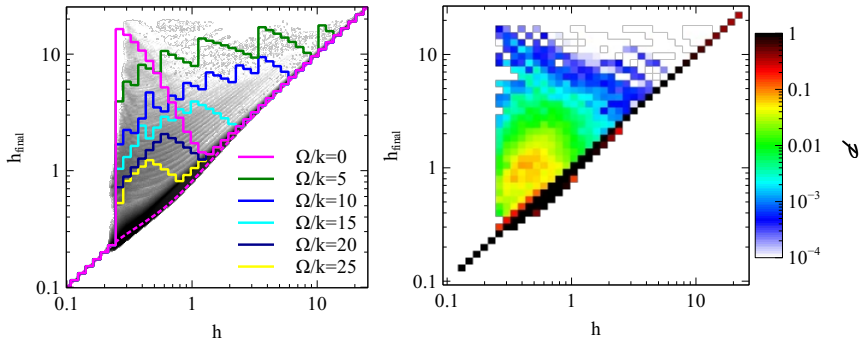

FIG. 10: Panel (a) shows analytical boundaries $\max h_{final}(h)$, $h - V(h)$ for several Ω/k values and averaged operator P from Fig. 9(b). Panel (b) shows analytically derived averaged operator P for uniform X distribution.

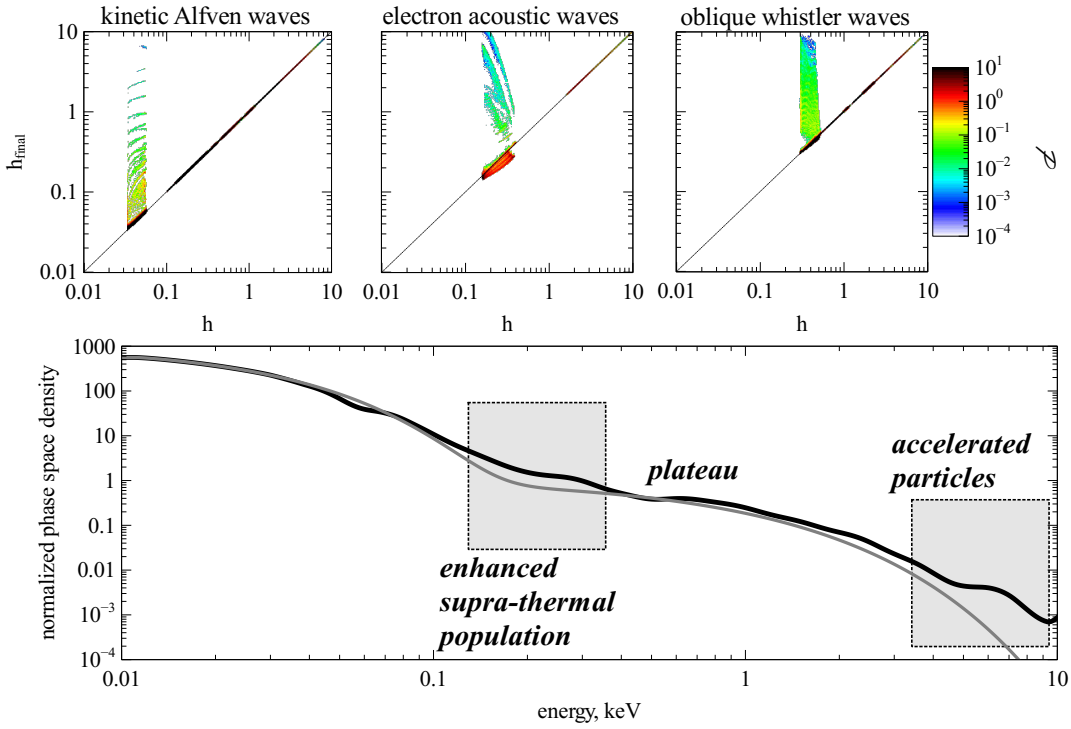

FIG. 11: Top panels show three operators P for wave modes form table I. Bottom panel shows the evolution of electron distribution function for ~ 100 interactions with wave-packets (~ 10 min for chosen system parameters, see details in the text).

applicability range of the proposed approach to a particular types of wave emission, the latter simplification is always satisfied for the Landau resonant interaction. Therefore, the obtained effects of the wave packet evolution on the particle resonant acceleration should exist for electromagnetic (e.g., whistler) wave as well [see, e.g., 46, 66, 67, 71–74], but the proposed approach is most appropriate for description of Landau resonance with very oblique whistler waves [e.g., 75], electron acoustic wave [e.g., 76], very oblique magnetosonic waves [e.g., 77], and ion acoustic waves [e.g., 78]. Moreover, using the proposed approach for the construction of an integral operator $\sim \mathcal{P}$ [see also 38, 79], one can in principle describe charged particle energization in various plasma systems (for waves with weak disoersiona nd small chipping). A different approach can be used to evaluate the effects of very short wave-packets representing the majority of intense parallel-propagating whistler-mode waves in the inner magnetosphere [80, 81], but averaged operators still need to be determined in this case, in the same manner as shown here. To demonstrate the applicability of the proposed approach for description of the wave-particle resonant interaction in space plasma, we consider three examples related to the inner Earth magnetosphere.

A resonant wave-particle interaction, in particular a nonlinear resonance characterized by particle phase trapping, is an important process determining charged particle energization in many space and laboratory plasma systems. Although an individual charged particle motion in the nonlinear resonance is well described theoretically, the kinetic equation modeling the long-term evolution of the resonant particle ensemble has been developed only recently. The present study is devoted to generalization of this equation for systems with localized wave packets propagating with the wave group velocity different from the wave phase velocity. We demonstrate how wave-packet properties determine the efficiency of resonant particle acceleration and derive the nonlocal integral operator acting on the resonant particle distribution. This operator describes particle distribution variations due to interaction with one wave-packet. We solve kinetic equation with this operator for many wave-packets and show that solutions coincide with the results of the numerical integration of test particle trajectories. Applications of the proposed approach to description of space plasma systems are discussed.

The Landau resonance of nonrelativistic electrons and localized wave packets of oblique whistler waves, electron acoustic waves, and kinetic Alfven waves represent an important example of nonrelativistic electron acceleration in the near-Earth plasma environment. These three wave modes are exited at the fast plasma flows penetrating the inner Earth magnetosphere [14, 82–84] and can significantly affect the thermal electrons transported by these flows [85–87]. Electron acoustic waves represent purely electrostatic wave mode [88]; kinetic Alfven waves and very oblique whistler waves are electromagnetic modes, but these waves carry a significant field-aligned electric field that resonate with electrons (and such resonant interaction is described by Hamiltonian (4), see details in [44, 89]). We consider evolution of a typical electron distribution observed within fast flows, $\Psi \sim (1 + h/h_0)^{-1} \exp(-h/h_0)$ with $h_0 \sim 1$ keV [e.g., 76, 83], due to resonant interaction with these three wave modes. Note, we assume (in agreement with spacecraft observations) that during a particular time interval (e.g., a time interval corresponding to fast plasma flows penetrating the inner Earth magnetosphere) different wave modes are generated and interact with electrons, but these waves are well separated in space and time and measured by spacecraft (and presumably seen by particles) as non-overlapping wave-packets (i.e., there is no resonance overlapping, otherwise the resonant interaction would be reduced to diffusion-like interaction [see, e.g., 34, 35]).

There are several important wave characteristics defining such resonant interaction: wave phase velocity v_ϕ (we use the parameter $h_\phi = v_\phi m_e/2h_0$), dimensionless wave number $kR = \omega R/v_\phi$, number of wavelengths, N, within the wave-packet, typical amplitude of the wave field-aligned electric field E_0 (we use the dimensionless parameter $\varepsilon = -e\Phi_0/h_0 = (eRE_0/h_0)/kR$). Table I provides estimates of these parameters for wave modes observed by spacecraft in the inner Earth magnetopshere. Using these estimates, we construct three operators P with $\mathrm{X} = \delta(\Omega/k)$ for electron acoustic waves (these waves have almost linear dispersion), and uniform X for kinetic Alfven waves and oblique whistler waves. Figure 11(a) shows these three operators for electrons with intermediate pitch-angles ($\Omega_b^2 = 0.25$). Solution of Eq. (15) with a sum of these operators and initial distribution $\Psi \sim (1 + h/h_0)^{-1} \exp(-h/h_0)$ (we have also added a cold, of temperature $\sum h_0/25$, background always observed in the near-Earth plasma) is shown in Fig. 11(b). One can see three main effects of wave-particle resonant interaction. First, all three wave modes contribute to production of the high-energy population seen as a tail of the distribution ($h > 1$ keV). Such accelerated population is often measured by spacecraft around the plasma flows. Second, the competition of particle scattering and trapping (by electron acoustic waves and oblique whistler waves) results in formation of plateau around ~ 0.5 keV (energy range with very weak phase space density gradient). Such plateaus were observed around plasma flows and believed to be responsible for significant reduction of the Landau damping of electrostatic waves [e.g., 90]. Third, kinetic Alfven waves accelerate low-energy particles and enhance the population of $\sim 100 - 300$ eV electrons. Such enhancements were found before in self-consistent models of kinetic Alfven waves [45, 87]. Therefore, our simulation demonstrates that the proposed approach can be applied for description of realistic space plasma systems.

In conclusion, we have demonstrated and explained the effects of finite wave-packets and wave-packet evolution on trapping and acceleration of charged particles. A par-

wave mode	v_ϕ km/s	h_ϕ	kR	N mV/m	E_0	ε
KAW	10^3	10^{-2}	10^4	~ 5	10^{-1}	10^{-3}
EAW	10^4	0.3	10^3	~ 3	10	10^{-2}
OWW	10^4	0.3	$5 \cdot 10^3$	~ 25	1	10^{-3}

TABLE I: Characteristics of three wave modes observed by spacecraft in the inner magnetosphere (radial distance from the Earth $\sim 3 \cdot 10^4$ km; spatial scale of the magnetic field inhomogeneity is $R \sim 4 \cdot 10^4$ km) during plasma injections. Kinetic Alfven waves (KAW) propagate with the Alfven speed, carrying the field-aligned electric field ~ 0.1 mV/m, and occupy the frequency domain below ion cyclotron frequency [14, 82]. A typical KAW packet contains several wave lengths [9, 45]. Electron acoustic waves (EAW) propagate with the electron acoustic speed (defined by ratio of characteristics of cold and hot electron populations, see [88]), carrying very strong field-aligned field [6, 76], and have a typical frequency (ratio of wavelength and phase velocity) about a fraction of the electron cyclotron frequency [84, 91]. These waves quickly evolve into very localized wave-packets containing few (or even a single) wave length [76, 85]. Oblique whistler waves (OWW) propagate in a form of wave-packets containing tens of wave lengths and carry the field-aligned electric field about $1 - 10$ mV/m [13, 75].

ticle accelerates due to a trapping into the resonance and the subsequent escape from the resonance (a detrapping), whereas scatterings result in particle deceleration. The wave-packet evolution alter the particle energy gain between a trapping and the following detrapping. We have shown that effects of acceleration (due to trapping) and deceleration (due to scattering) can be included into the kinetic equation through an integral operator. Such an operator has been evaluated numerically and shown to satisfy the main property of the trapping/scattering relation ($\Pi = -dV/dh$) for the simplest case of a single resonant interaction with an non-evolving wave-packet. Operators constructed for more complicated systems (including many resonant interactions and wave-packet evolution) do not follow the $\Pi = -dV/dh$ equation over the entire energy range of resonant particles. We have demonstrated that solutions of the kinetic equation including these operators describe well the evolution of the resonant particle distribution.

ACKNOWLEDGMENTS

The work was supported by the Russian Scientific Fund, project # 14-12-00824.

[1] H. Matsumoto, H. Kojima, T. Miyatake, Y. Omura, M. Okada, I. Nagano, and M. Tsutsui, Geophys. Res. Lett. **21**, 2915 (1994).
[2] S. D. Bale, P. J. Kellogg, D. E. Larsen, R. P. Lin, K. Goetz, and R. P. Lepping, Geophys. Res. Lett. **25**, 2929 (1998).
[3] R. E. Ergun, D. M. Malaspina, I. H. Cairns, M. V. Goldman, D. L. Newman, P. A. Robinson, S. Eriksson, J. L. Bougeret, C. Briand, S. D. Bale, C. A. Cattell, P. J. Kellogg, and M. L. Kaiser, Physical Review Letters **101**, 051101 (2008).
[4] R. E. Ergun, L. Andersson, J. Tao, V. Angelopoulos, J. Bonnell, J. P. McFadden, D. E. Larson, S. Eriksson, T. Johansson, C. M. Cully, D. N. Newman, M. V. Goldman, A. Roux, O. Lecontel, K.-H. Glassmeier, and W. Baumjohann, Physical Review Letters **102**, 155002 (2009).
[5] F. S. Mozer, O. Agapitov, V. Krasnoselskikh, S. Lejosne, G. D. Reeves, and I. Roth, Physical Review Letters **113**, 035001 (2014).
[6] F. S. Mozer, O. Agapitov, A. Artemyev, J. F. Drake, V. Krasnoselskikh, S. Lejosne, and I. Vasko, Geophys. Res. Lett. **42**, 3627 (2015).
[7] D. M. Malaspina, J. R. Wygant, R. E. Ergun, G. D. Reeves, R. M. Skoug, and B. A. Larsen, J. Geophys. Res. **120**, n/a (2015), 2015JA021137.
[8] A. V. Artemyev, R. Rankin, and I. Y. Vasko, J. Geophys. Res. **122**, 5519 (2017).
[9] J. R. Wygant, A. Keiling, C. A. Cattell, R. L. Lysak, M. Temerin, F. S. Mozer, C. A. Kletzing, J. D. Scudder, V. Streltsov, W. Lotko, and C. T. Russell, J. Geophys. Res. **107**, 1201 (2002).
[10] C. Cattell, J. R. Wygant, K. Goetz, K. Kersten, P. J. Kellogg, T. von Rosenvinge, S. D. Bale, I. Roth, M. Temerin, M. K. Hudson, R. A. Mewaldt, M. Wiedenbeck, M. Maksimovic, R. Ergun, M. Acuna, and C. T. Russell, Geophys. Res. Lett. **35**, L01105 (2008).
[11] L. B. Wilson, III, C. A. Cattell, P. J. Kellogg, J. R. Wygant, K. Goetz, A. Breneman, and K. Kersten, Geophys. Res. Lett. **38**, L17107 (2011).
[12] Y. V. Khotyaintsev, C. M. Cully, A. Vaivads, M. André, and C. J. Owen, Physical Review Letters **106**, 165001 (2011).
[13] O. Agapitov, A. Artemyev, D. Mourenas, V. Krasnoselskikh, J. Bonnell, O. Le Contel, C. M. Cully, and V. Angelopoulos, J. Geophys. Res. **119**, 1606?1626 (2014).
[14] D. M. Malaspina, S. G. Claudepierre, K. Takahashi, A. N. Jaynes, S. R. Elkington, R. E. Ergun, J. R. Wygant, G. D. Reeves, and C. A. Kletzing, Geophys. Res. Lett. **42**, 9203 (2015).
[15] J. E. Fahlen, B. J. Winjum, T. Grismayer, and W. B. Mori, Physical Review Letters **102**, 245002 (2009).
[16] B. Van Compernolle, X. An, J. Bortnik, R. M. Thorne, P. Pribyl, and W. Gekelman, Physical Review Letters **114**, 245002 (2015).
[17] E. M. Tejero, C. Crabtree, D. D. Blackwell, W. E. Am-

atucci, M. Mithaiwala, G. Ganguli, and L. Rudakov, Scientific Reports **5**, 17852 (2015).
[18] M. E. Viktorov, S. V. Golubev, D. A. Mansfeld, and A. V. Vodopyanov, AIP Conference Proceedings **1771**, 070010 (2016).
[19] V. D. Shapiro and R. Z. Sagdeev, Physics Reports **283**, 49 (1997).
[20] J. M. Albert, X. Tao, and J. Bortnik, in *Dynamics of the Earth's Radiation Belts and Inner Magnetosphere*, American Geophysical Union, edited by D. Summers, I. U. Mann, D. N. Baker, and M. Schulz (2013).
[21] Y. Y. Shprits, D. A. Subbotin, N. P. Meredith, and S. R. Elkington, Journal of Atmospheric and Solar-Terrestrial Physics **70**, 1694 (2008).
[22] R. M. Thorne, Geophys. Res. Lett. **372**, L22107 (2010).
[23] I. Y. Dodin, Fusion Science and Technology **65**, 54 (2014).
[24] D. Bénisti, Physics of Plasmas **24**, 092120 (2017), arXiv:1706.03540 [physics.plasm-ph].
[25] R. M. Thorne, B. Ni, X. Tao, R. B. Horne, and N. P. Meredith, Nature (London) **467**, 943 (2010).
[26] R. M. Thorne, W. Li, B. Ni, Q. Ma, J. Bortnik, L. Chen, D. N. Baker, H. E. Spence, G. D. Reeves, M. G. Henderson, C. A. Kletzing, W. S. Kurth, G. B. Hospodarsky, J. B. Blake, J. F. Fennell, S. G. Claudepierre, and S. G. Kanekal, Nature (London) **504**, 411 (2013).
[27] A. Y. Ukhorskiy, M. I. Sitnov, D. G. Mitchell, K. Takahashi, L. J. Lanzerotti, and B. H. Mauk, Nature (London) **507**, 338 (2014).
[28] Y. Y. Shprits, A. Y. Drozdov, M. Spasojevic, A. C. Kellerman, M. E. Usanova, M. J. Engebretson, O. V. Agapitov, I. S. Zhelavskaya, T. J. Raita, H. E. Spence, D. N. Baker, H. Zhu, and N. A. Aseev, Nature Communications **7**, 12883 (2016).
[29] W. E. Drummond and D. Pines, Nuclear Fusion Suppl. **3**, 1049 (1962).
[30] A. A. Vedenov, E. Velikhov, and R. Sagdeev, Nuclear Fusion Suppl. **2**, 465 (1962).
[31] C. F. Kennel and F. Engelmann, Physics of Fluids **9**, 2377 (1966).
[32] X. Tao, J. Bortnik, J. M. Albert, and R. M. Thorne, J. Geophys. Res. **117**, A10205 (2012).
[33] J. M. Albert, J. Geophys. Res. **115**, A00F05 (2010).
[34] E. Nagornykh and A. Tel'nikhin, in *Plasma Physics*, American Institute of Physics Conference Series, Vol. 669, edited by I. S. Falconer, R. L. Dewar, and J. Khachan (2003) pp. 824–827 .
[35] G. V. Khazanov, A. A. Tel'nikhin, and T. K. Kronberg, Nonlinear Processes in Geophysics **21**, 61 (2014) .
[36] A. V. Artemyev, A. I. Neishtadt, A. A. Vasiliev, and D. Mourenas, Physics of Plasmas **23**, 090701 (2016).
[37] N. Furuya, Y. Omura, and D. Summers, J. Geophys. Res. **113**, A04224 (2008).
[38] Y. Omura, Y. Miyashita, M. Yoshikawa, D. Summers, M. Hikishima, Y. Ebihara, and Y. Kubota, J. Geophys. Res. **120**, 9545 (2015).
[39] A. V. Artemyev, A. I. Neishtadt, A. A. Vasiliev, and D. Mourenas, Phys. Rev. E **95**, 023204 (2017).
[40] A. V. Artemyev, A. I. Neishtadt, A. A. Vasiliev, and D. Mourenas, Journal of Plasma Physics **84**, 905840206 (2018).
[41] I. Y. Vasko, O. V. Agapitov, F. S. Mozer, and A. V. Artemyev, J. Geophys. Res. **120**, 8616 (2015).
[42] F. S. Mozer, A. Artemyev, O. V. Agapitov, D. Mourenas, and I. Vasko, Geophys. Res. Lett. **43**, 508 (2016).
[43] C. E. J. Watt and R. Rankin, Physical Review Letters **102**, 045002 (2009).
[44] A. V. Artemyev, R. Rankin, and M. Blanco, J. Geophys. Res. **120**, 10 (2015).
[45] P. A. Damiano, J. R. Johnson, and C. C. Chaston, J. Geophys. Res. **121**, 10,831 (2016).
[46] Y. Kubota and Y. Omura, J. Geophys. Res. **123**, 4835,.
[47] D. Bénisti, O. Morice, L. Gremillet, A. Friou, and E. Lefebvre, Physics of Plasmas **19**, 056301 (2012).
[48] P. Michel, L. Divol, E. L. Dewald, J. L. Milovich, M. Hohenberger, O. S. Jones, L. B. Hopkins, R. L. Berger, W. L. Kruer, and J. D. Moody, Physical Review Letters **115**, 055003 (2015).
[49] E. L. Dewald, F. Hartemann, P. Michel, J. Milovich, M. Hohenberger, A. Pak, O. L. Landen, L. Divol, H. F. Robey, O. A. Hurricane, T. Döppner, F. Albert, B. Bachmann, N. B. Meezan, A. J. MacKinnon, D. Callahan, and M. J. Edwards, Physical Review Letters **116**, 075003 (2016).
[50] J. R. Cary and A. J. Brizard, Reviews of Modern Physics **81**, 693 (2009).
[51] J. M. Albert, Physics of Fluids B **5**, 2744 (1993).
[52] D. Shklyar and H. Matsumoto, Surveys in Geophysics **30**, 55 (2009).
[53] D. R. Shklyar, Sov. Phys. JETP **53**, 1197 (1981).
[54] T. G. Northrop, *The adiabatic motion of charged particles* (Interscience Publishers John Wiley and Sons, New York-London-Sydney, 1963).
[55] D. L. Bruhwiler and J. R. Cary, Physical Review Letters **68**, 255 (1992).
[56] S. K. Matsoukis, S. Chapman, and G. Rowlands, Physica D Nonlinear Phenomena **138**, 251 (2000).
[57] W. J. Wykes, S. C. Chapman, and G. Rowlands, Physics of Plasmas **8**, 2953 (2001).
[58] A. I. Neishtadt and A. A. Vasiliev, Nuclear Instruments and Methods in Physics Research A **561**, 158 (2006), arXiv:nlin/0511050.
[59] A. I. Neishtadt, Russian Mathematical Surveys **69**, 771 (2014).
[60] A. I. Neishtadt, in Hamiltonian Systems with Three or More Degrees of Freedom, ed. Simo C., NATO ASI Series C. Dordrecht: Kluwer Acad. Publ. **533**, 193 (1999).
[61] A. P. Itin, A. I. Neishtadt, and A. A. Vasiliev, Physica D: Nonlinear Phenomena **141**, 281 (2000).
[62] A. Vasiliev, A. Neishtadt, and A. Artemyev, Physics Letters A **375**, 3075 (2011).
[63] A. V. Artemyev, A. A. Vasiliev, D. Mourenas, O. Agapitov, and V. Krasnoselskikh, Physics of Plasmas **20**, 122901 (2013).
[64] N. G. Van Kampen, *Stochastic Processes in Physics and Chemistry*, 3rd ed. (North Holland, 2003).
[65] D. Vainchtein, G. Fridman, and A. Artemyev, Communications in Nonlinear Science and Numerical Simulations **51**, 133 (2017).
[66] Y. Katoh and Y. Omura, J. Geophys. Res. **109**, A12214 (2004).
[67] J. Bortnik, R. M. Thorne, and U. S. Inan, Geophys. Res. Lett. **35**, L21102 (2008).
[68] Y.-K. Hsieh and Y. Omura, J. Geophys. Res. **122**, 675 (2017).
[69] A. V. Artemyev, A. A. Vasiliev, D. Mourenas, A. I. Neishtadt, O. V. Agapitov, and V. Krasnoselskikh, Physics of Plasmas **22**, 112903 (2015).

[70] C. Crabtree, G. Ganguli, and E. Tejero, Physics of Plasmas **24**, 056501 (2017).

[71] A. G. Demekhov, V. Y. Trakhtengerts, M. J. Rycroft, and D. Nunn, Geomagnetism and Aeronomy **46**, 711 (2006).

[72] A. G. Demekhov, V. Y. Trakhtengerts, M. Rycroft, and D. Nunn, Geomagnetism and Aeronomy **49**, 24 (2009).

[73] A. Osmane and A. M. Hamza, Nonlinear Processes in Geophysics **21**, 115 (2014), arXiv:1402.1691 [physics.space-ph].

[74] D. Nunn and Y. Omura, J. Geophys. Res. **120**, 2890 (2015).

[75] A. Artemyev, O. Agapitov, D. Mourenas, V. Krasnoselskikh, V. Shastun, and F. Mozer, Space Science Reviews **200**, 261 (2016).

[76] I. Y. Vasko, O. V. Agapitov, F. S. Mozer, J. W. Bonnell, A. V. Artemyev, V. V. Krasnoselskikh, G. Reeves, and G. Hospodarsky, Geophys. Res. Lett. **44**, 4575 (2017).

[77] A. V. Artemyev, D. Mourenas, O. V. Agapitov, and V. V. Krasnoselskikh, Physics of Plasmas **22**, 062901 (2015).

[78] L. B. Wilson, III, C. Cattell, P. J. Kellogg, K. Goetz, K. Kersten, L. Hanson, R. MacGregor, and J. C. Kasper, Physical Review Letters **99**, 041101 (2007).

[79] Y.-K. Hsieh and Y. Omura, Radio Science **52**, 1268 (2017), 2017RS006245.

[80] D. Mourenas, X.-J. Zhang, A. V. Artemyev, V. Angelopoulos, R. M. Thorne, J. Bortnik, A. I. Neishtadt, and A. A. Vasiliev, J. Geophys. Res. **123**, 4979 (2018).

[81] X.-J. Zhang, R. Thorne, A. Artemyev, D. Mourenas, V. Angelopoulos, J. Bortnik, C. A. Kletzing, W. S. Kurth, and G. B. Hospodarsky, J. Geophys. Res. **123**, 5379,.

[82] C. C. Chaston, J. W. Bonnell, L. Clausen, and V. Angelopoulos, J. Geophys. Res. **117**, A09202 (2012).

[83] I. Y. Vasko, O. V. Agapitov, F. S. Mozer, J. W. Bonnell, A. V. Artemyev, V. V. Krasnoselskikh, and Y. Tong, Physical Review Letters **120**, 195101 (2018).

[84] D. M. Malaspina, A. Ukhorskiy, X. Chu, and J. Wygant, J. Geophys. Res. **123**, 2566 (2018).

[85] O. Agapitov, J. F. Drake, I. Vasko, F. S. Mozer, A. Artemyev, V. Krasnoselskikh, V. Angelopoulos, J. Wygant, and G. D. Reeves, Geophys. Res. Lett. **45**, 2168 (2018).

[86] I. Y. Vasko, V. V. Krasnoselskikh, F. S. Mozer, and A. V. Artemyev, Physics of Plasmas **25**, 072903 (2018).

[87] P. A. Damiano, C. C. Chaston, A. J. Hull, and J. R. Johnson, Geophys. Res. Lett. **45**, 5826 (2018).

[88] S. P. Gary and R. L. Tokar, Physics of Fluids **28**, 2439 (1985).

[89] A. Artemyev, V. Krasnoselskikh, O. Agapitov, D. Mourenas, and G. Rolland, Physics of Plasmas **19**, 122901 (2012).

[90] W. Li, D. Mourenas, A. V. Artemyev, J. Bortnik, R. M. Thorne, C. A. Kletzing, W. S. Kurth, G. B. Hospodarsky, G. D. Reeves, H. O. Funsten, and H. E. Spence, Geophys. Res. Lett. **43**, 8867 (2016).

[91] I. Y. Vasko, O. V. Agapitov, F. S. Mozer, A. V. Artemyev, J. F. Drake, and I. V. Kuzichev, J. Geophys. Res. **122**, 120 (2017).